THE JOURNAL OF BIOLOGICAL CHEMISTRY VOL. 290, NO. 31, pp. 19334–19342, July 31, 2015

Fluorinated Aromatic Amino Acids Distinguish Cation-π Interactions from Membrane Insertion*

Received for publication, May 29, 2015, and in revised form, June 16, 2015 Published, JBC Papers in Press, June 19, 2015, DOI 10.1074/jbc.M115.668343

Tao He[‡], **Anne Gershenson**[§], **Stephen J. Eyles**[§], **Yan-Jiun Lee**[¶], **Wenshe R. Liu**[¶], **Jiangyun Wang**[||], **Jianmin Gao**[‡], **and Mary F. Roberts**[‡1]

From the [‡]*Department of Chemistry, Boston College, Chestnut Hill, Massachusetts 02467,* [§]*Department of Biochemistry and Molecular Biology, University of Massachusetts Amherst, Amherst, Massachusetts 01003,* [¶]*Department of Chemistry, Texas A&M University, College Station, Texas 77843, and* [||]*Institute of Biophysics, Chinese Academy of Sciences, Chaoyang District, Beijing 100101, China*

Background: Peripheral membrane proteins can interact with zwitterionic phospholipid headgroups or lipid tails.
Results: Incorporation of fluorinated Phe or Tyr differentiates side chain insertion from PC-cation-π complexes.
Conclusion: Enhanced binding of a fluorinated protein implies side chain insertion; weakened binding represents a cation-π complex.
Significance: Fluorinated Tyr or Phe incorporation can elucidate membrane binding modes.

Cation-π interactions, where protein aromatic residues supply π systems while a positive-charged portion of phospholipid head groups are the cations, have been suggested as important binding modes for peripheral membrane proteins. However, aromatic amino acids can also insert into membranes and hydrophobically interact with lipid tails. Heretofore there has been no facile way to differentiate these two types of interactions. We show that specific incorporation of fluorinated amino acids into proteins can experimentally distinguish cation-π interactions from membrane insertion of the aromatic side chains. Fluorinated aromatic amino acids destabilize the cation-π interactions by altering electrostatics of the aromatic ring, whereas their increased hydrophobicity enhances membrane insertion. Incorporation of pentafluorophenylalanine or difluorotyrosine into a *Staphylococcus aureus* phosphatidylinositol-specific phospholipase C variant engineered to contain a specific PC-binding site demonstrates the effectiveness of this methodology. Applying this methodology to the plethora of tyrosine residues in *Bacillus thuringiensis* phosphatidylinositol-specific phospholipase C definitively identifies those involved in cation-π interactions with phosphatidylcholine. This powerful method can easily be used to determine the roles of aromatic residues in other peripheral membrane proteins and in integral membrane proteins.

Membrane binding by peripheral membrane proteins is often mediated by specific recognition of a variety of anionic phospholipids (*e.g.* phosphatidylserine (1), phosphoinositides (2, 3), phosphatidic acid (4)). Although phosphatidylcholine (PC),[2] a major component of eukaryotic membranes, is usually considered a structural lipid, it can also serve as a specific anchor for peripheral membrane proteins. For example, the extracellular *Bacillus thuringiensis* virulence factor phosphatidylinositol-specific phospholipase C binds poorly to vesicles composed of anionic phospholipids at physiological salt concentrations but shows increasing avidity for vesicles containing PC (5). The targets of this enzyme are glycosylphosphatidylinositol-anchored proteins in the external leaflet of the plasma membrane, and affinity for PC would aid in directing the enzyme to its mammalian cell target. Mutagenesis (6), NMR (7), and molecular dynamics (MD) (6) simulations are consistent with choline cation-tyrosine π complexes providing a significant amount of the binding energy for *B. thuringiensis* PI-PLC. However, none of these experiments absolutely distinguishes nonspecific side-chain insertion from very specific formation of a cation-π complex with PC. The cation-π complex is formed above the hydrocarbon boundary in the hydrated part of the phospholipid, whereas membrane insertion places the side chain into the hydrocarbon portion. Substitution of alanine in place of tyrosine produces a large change in the side chain volume and, therefore, cannot identify the source of lost binding affinity. NMR experiments can localize long-lived PC binding sites but cannot define the binding mechanism. In contrast, such complexes can be identified in MD simulations, but many are transient in nature and may or may not be populated when the protein interacts with membranes. Clearly, a more direct experimental method is needed to demonstrate the existence of such interactions.

We have developed a method to separate the two membrane binding modes using site-specific incorporation of fluorinated amino acids, in this case pentafluorophenylalanine (F-F_5) and 3,5-difluorotyrosine (Y-F_2). The fluorinated amino acids are

* This work was supported, in whole or in part, by National Institutes of Health Grant 60418 (to M. F. R.).
The atomic coordinates and structure factors (codes 4S3G and 4RV3) have been deposited in the Protein Data Bank (http://wwpdb.org/).
[1] To whom correspondence should be addressed: Dept. of Chemistry, Boston College, Merkert Chemistry Center, 2609 Beacon Street, Chestnut Hill, MA 02467. Tel.: 617-552-3616; Fax: 617-552-2705; E-mail: mary.roberts@bc.edu.

[2] The abbreviations used are: PC, phosphatidylcholine; PG, phosphatidylglycerol; F-F_5, pentafluorophenylalanine; Y-F_2, 3,5-difluorotyrosine; PI-PLC, phosphatidylinositol (PI)-specific phospholipase C; SUV, small unilamellar vesicle; FCS, fluorescence correlation spectroscopy; ESI, electrospray ionization; X_{PC}, mole fraction PC.

more hydrophobic (8) and are, therefore, likely to enhance binding by insertion. However, the altered electrostatics of the fluorinated aromatic ring should destabilize cation-π interactions (9).

The method is first tested with the extracellular *Staphylococcus aureus* PI-PLC, which has little affinity for PC and binds preferentially to membranes rich in anionic phospholipids (10, 11). However, the introduction of two tyrosines at Asn-254 and His-258 (N254Y/H258Y), to mimic the *Bacillus* enzyme, leads to PC binding specificity, presumably due to the cation-π complexes observed in a crystal structure of N254Y/H258Y with a dibutyroyl-PC bound (12). In contrast, a phenylalanine (Phe-249) in a surface loop around the *S. aureus* PI-PLC active site is thought to contribute to binding by inserting into the membrane (9, 10). A fluorinated Tyr at residue 258 weakens protein binding to PC-rich vesicles, confirming the importance of choline cation-Tyr π interactions at this site, whereas a fluorinated Phe at 249 enhances vesicle binding for all vesicle compositions indicating nonspecific hydrophobic interactions with lipid tails. With this confirmation that the methodology works as predicted, the many surface Tyr of *B. thuringiensis* PI-PLC were replaced with 3,5-difluotoryrosine to determine which Tyr residues are involved in cation-π interactions with PC. This method for determining how aromatic residues interact with phospholipids is readily applicable to other peripheral membrane proteins.

EXPERMENTAL PROCEDURES

Chemicals—F-F_5 was prepared by one-step deprotection of the commercially available *t*-butoxycarbonyl-L-pentafluorophenylalanine. Y-F_2 was synthesized following established methods (13).

Preparation and Characterization of Fluorinated PI-PLC Enzymes—To site-specifically incorporate these two unnatural amino acids into *S. aureus* PI-PLC, pEVOL-pylT-PylRS and pEVOL-F2YRS (14) were used. Although broadly similar to the system to incorporate Y-F_2, the full characterization of pEVOL-pylT-PylRS for F-F_5 incorporation will be described in a separate report. These plasmids each contain a tRNA-tRNA synthetase pair evolved for the incorporation of F-F_5 or Y-F_2, respectively. An amber stop codon was substituted at specific sites in *S. aureus* PI-PLC gene for incorporation of the fluorinated amino acid at the desired position. To express fluorinated mutants F249F-F_5, H258F-F_5, and N254Y/H258Y-F_2, the mutant plasmids and the appropriate pEVOL (15) plasmid were cotransformed into *Escherichia coli* BL21(DE3) (10). Proteins were purified by chromatography using a nickel-nitrilotriacetic acid affinity resin and then an anion exchange resin, as described previously for this protein and its variants (11, 12).

A previously described *B. thuringiensis* PI-PLC plasmid (16) was subcloned into the pET-23b vector to create a C-terminal His tag. A similar expression and purification procedure was used for incorporation of Y-F_2 into *B. thuringiensis* PI-PLC to generate Y86Y-F_2, Y88Y-F_2, Y204Y-F_2, Y246Y-F_2, Y247Y-F_2, Y248Y-F_2, and Y251Y-F_2. However, the introduction of these fluorinated amino acids was done using N168C as the control. Fluorophores can be easily attached to this single Cys and have been shown to have minimal effect on enzyme activity or binding (5).

Mass Spectrometry—Samples were analyzed using instrumentation at the University of Massachusetts Mass Spectrometry Center. Samples were dissolved initially in water and then diluted to 1–10 μM in acetonitrile/water/acetic acid (50:47:3 v/v/v). Intact protein molecular weights were determined with a MicrOTOF II ESI-TOF mass spectrometer (Bruker Daltonics, Inc., Billerica MA) using electrospray ionization in positive mode. MS/MS data were obtained using a SolariX 7T FT-ICR (Bruker Daltonics) using collision-induced dissociation in the storage quadrupole (~5 V collision energy). The most intense charge state ion $[M+43H]^{43+}$ was selected for isolation. Although complete top-down fragmentation data were not obtained, representative fragments confirmed that fluorinated amino acids were correctly incorporated at the amber codon sites. Interestingly, the fluorinated analogs tended to fragment with a significantly lower (2–3 V) collision energy resulting in a quite different fragmentation pattern from the non-fluorinated version. This phenomenon will be the subject of future investigation.

MS analysis of tryptic peptides was required to identify the position of the Y-F_2 in *S. aureus* N254Y/H258Y-F_2. Tryptic peptides were also used to confirm the position of the fluorinated amino acid in H258F-F_5.

Enzyme Activity Assays—Enzymatic activities for all the *S. aureus* PI-PLC variants, determined toward 4 mM PI in small unilamellar vesicles (SUVs) with various amounts of PC, were measured by ^{31}P NMR spectroscopy as described previously (11, 12). The total phospholipid concentration of vesicles varied from 4 mM (mole fraction PC, $X_{PC} = 0$) to 20 mM ($X_{PC} = 0.8$). The assay buffer was 50 mM MES, pH 6.5.

Vesicle Binding Assays—Fluorescence correlation spectroscopy (FCS) was used to measure binding of the control proteins and their fluorinated counterparts to PG/PC SUVs. The *S. aureus* proteins were labeled on the N-terminal amino groups with Alexa Fluor 488 succinimidyl ester (11, 12). Vesicle binding of these proteins (3.5 nM) to SUVs composed of PG (the substrate analog) and PC, prepared by sonication, was measured at pH 6.5 (in 50 mM MES containing 1 mg/ml BSA), the optimum pH for enzyme activity (11). For FCS experiments with the *B. thuringiensis* PI-PLC, all Y-Y_2 mutants also contained N168C, which was covalently labeled with Alexa Fluor 488 maleimide (5). *B. thuringiensis* PI-PLC proteins at 10 nM were in phosphate-buffered saline, pH 7.4, with 1 mg/ml BSA for titrations with the PG/PC SUVs.

The FCS measurements were carried out at 22 °C using a home-built confocal setup based on an IX-70 inverted microscope. Details of the experimental set-up and data analysis have been previously described (6, 17). Proteins were titrated with SUVs, and the fraction of protein bound to vesicles was determined from two species fits to the autocorrelations (obtained in cross-correlation mode), $G(\tau) = A_p g_p(\tau) + A_v g_v(\tau)$, where p and v denote free protein and SUVs that are fluorescent due to PI-PLC binding, respectively, and A is the amplitude of species p and v (18–20). The dependence of the fraction protein bound on total phospholipid concentration was used to extract an apparent K_d.

Crystallization—Purified PI-PLC variants were concentrated to 20 mg/ml and then combined with *myo*-inositol (100 mM). The protein solution was then diluted to 10 mg/ml using

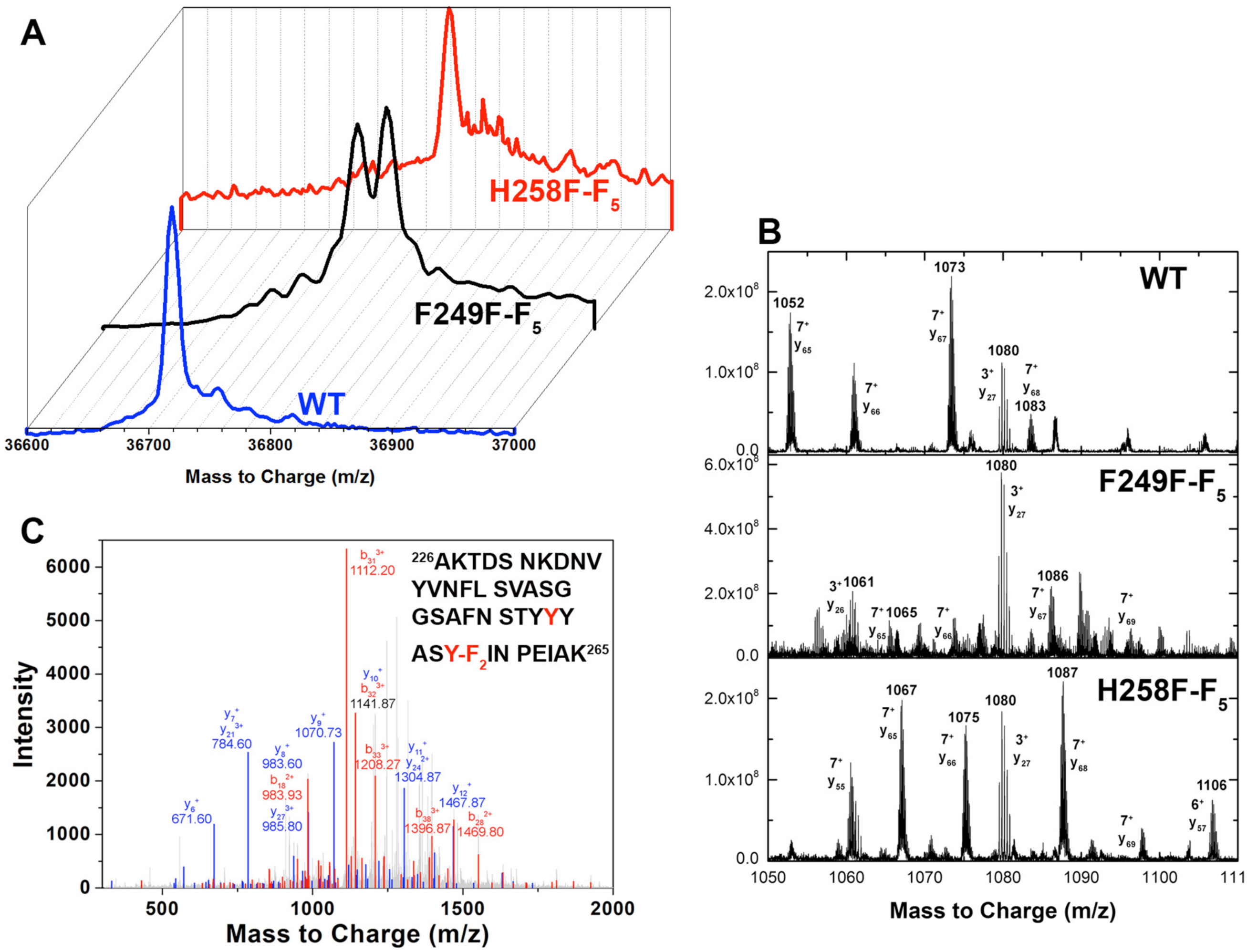

FIGURE 1. **MS confirmation of fluorinated amino acid incorporation in *S. aureus* PI-PLC.** *A*, intact MS analysis of wild type, F249F-F_5, and H258F-F_5 *S. aureus* PI-PLC variants. *B*, MS/MS analysis of *S. aureus* PI-PLC, F249F-F_5, and H258F-F_5. *C*, MS/MS identification of the tryptic peptide fragments containing the fluorinated tyrosine in N254Y/H258Y-F_2. *Red* and *blue* indicate the b (N-terminal) and y (C-terminal) ions, respectively. The peptide amino acid sequence is shown in the *upper right* with the mutations N254Y and H258Y-F_2 indicated in *red*.

deionized water and incubated on ice for a minimum of 2 h before setting up crystallization trays. The PI-PLC samples were crystallized at 4 °C by vapor diffusion using hanging drops of 3 μl at a final protein concentration of 10 mg/ml. For both mutants, the protein crystallized in 150 mM ammonium acetate, 100 mM sodium acetate, pH 4.6, with 10 mM magnesium nitrate and 20–24% PEG 4000.

Crystallography—Data were collected at 100 K using a Rigaku MicroMax-07 HF high intensity microfocus rotating copper anode x-ray generator coupled with Osmic VariMax Optics and a R-Axis IV++ image plate area detector. Data were indexed and reduced using d*TREK (21). Both structures were solved by molecular replacement in PHENIX (22) using PHASER (23) in PHENIX with the *S. aureus* structure 3V18 as a model. All models were refined with Phenix.refine, with manual model building in COOT (24). Maps were generated in PHENIX. Structural comparisons were made using SSM superposition (25) in COOT and alignment in PyMOL (26).

Results and Discussion

Incorporation of F-F_5 and Y-F_2 into S. aureus PI-PLC—ESI-TOF MS analysis was used to show that the fluorinated amino acids were properly incorporated into *S. aureus* PI-PLC F249F-F_5 and H258F-F_5. F249F-F_5 gave an observed average mass of 36,807 Da, and H258F-F_5 gave an average mass of 36,819 Da, whereas wild type had an observed mass of 36,719 Da (Fig. 1). These results are in agreement with the calculated mass. MS/MS analysis also confirmed the fluorinated modification at these desired sites (Fig. 1*B*). Thus, the ESI-MS and MS/MS together confirmed successful incorporation of F-F_5 at sites 249 and 258 using the cloning and expression strategies described. The N254Y/H258Y-F_2 variant showed a high avidity for salt, making it difficult to desalt the sample sufficiently for MS analysis, precluding successful analysis by ESI-TOF. Instead, the protein containing Y-F_2 was trypsinized, and the mixture was examined for fluorinated peptides to determine the site of fluoro-amino acid incorporation. Fig. 1*C* shows the ions corresponding to fragments of the tryptic peptide containing Y-F_2 at residue 258 in *S. aureus* PI-PLC. The MS/MS fragments detected for relevant peptides in both N254Y/H258Y-F_2 and H258F-F_5 are provided in Tables 1 and 2, confirming the successful incorporation of the fluorinated amino acids.

TABLE 1

MS/MS fragments of the tryptic peptide containing the N254Y/H258Y-F$_2$ mutation with intensities >900

The full peptide sequence is ^{226}AKTDS NKDNVYVNFL SVASGGSAFN STYYYAS **Y-F$_2$**IN PEIAK^{265} and the MS/MS data, including all identified peptides, are shown in Fig. 1*C*.

	Fragment sequence	Predicted mass	Measured mass
		Da	*Da*
C-terminal fragment			
y_6^+	^{260}N PEIAK^{265}	671.37	671.60
y_7^+	^{259}IN PEIAK^{265}	784.46	784.60
y_8^+	^{258} **Y-F$_2$** IN PEIAK^{265}	983.50	983.60
y_9^+	^{257}S**Y-F$_2$**IN PEIAK^{265}	1070.53	1070.73
y_{10}^+	^{256}AS **Y-F$_2$**IN PEIAK^{265}	1141.57	1141.87
y_{11}^+	^{255}YAS**Y-F$_2$**IN PEIAK^{265}	1304.63	1304.87
y_{12}^+	^{254}**Y**YAS**Y-F$_2$**IN PEIAK^{265}	1467.70	1467.87
y_{21}^{3+}	^{245}GGSAFN STY**Y**YAS**Y-F$_2$**IN PEIAK^{265}	784.69	784.60
y_{24}^{2+}	^{242}VASGGSAFN STY**Y**YAS**Y-F$_2$**IN PEIAK^{265}	1305.10	1304.87
y_{27}^{3+}	^{239}FLSVASGGSAFNSTY**Y**YAS**Y-F$_2$**IN PEIAK^{265}	986.13	985.80
N-terminal fragment			
b_{18}^{2+}	^{226}AKTDS NKDNVYVNFL SVA^{242}	983.99	983.93
b_{28}^{2+}	^{226}AKTDSNKDNVYVNFLSVASGGSAFN STY^{253}	1469.69	1469.80
b_{31}^{3+}	^{226}AKTDS NKDNVYVNFL SVASGGSAFN STY**Y**YA^{256}	1112.52	1112.20
b_{32}^{3+}	^{226}AKTDS NKDNVYVNFL SVASGGSAFN STY**Y**YAS^{257}	1141.53	1141.87
b_{33}^{3+}	^{226}AKTDS NKDNVYVNFL SVASGGSAFN STY**Y**YAS **Y-F$_2$**^{258}	1207.88	1208.27
b_{38}^{3+}	^{226}AKTDS NKDNVYVNFL SVASGGSAFNSTY**Y** YAS **Y-F$_2$**IN PEI^{263}	1396.64	1396.87

TABLE 2

MS/MS fragments of the tryptic peptide containing the H258F-F$_5$ mutation

The full peptide sequence is ^{226}AKTDS NKDNVYVNFL SVASGGSAFN STYN-YAS**F-F$_5$**IN PEIAK^{265}, and the MS/MS data are shown in Fig. 1.

C-terminal fragment	Fragment sequence	Predicted mass	Measured mass
		Da	*Da*
y_5^+	^{261}PEIAK^{265}	557.33	557.33
y_6^+	^{260}N PEIAK^{265}	671.37	671.40
y_7^+	^{259}IN PEIAK^{265}	784.46	784.47
y_8^+	^{258}**F-F$_5$**IN PEIAK^{265}	1021.48	1021.47
y_9^+	^{257}S**F-F$_5$**IN PEIAK^{265}	1108.51	1108.60
y_{10}^+	^{256}AS**F-F$_5$**IN PEIAK^{265}	1179.55	1179.60
y_{11}^+	^{255}YAS**F-F$_5$**IN PEIAK^{265}	1342.61	1342.60
y_{12}^+	^{254}NYAS**F-F$_5$**IN PEIAK^{265}	1456.65	1456.60
y_{13}^+	^{253}YNYAS**F-F$_5$**IN PEIAK^{265}	1619.72	1619.73
y_{15}^+	^{251}STYNYAS**F-F$_5$**IN PEIAK^{265}	1807.80	1807.40
y_{16}^+	^{250}N STYNYAS**F-F$_5$**IN PEIAK^{265}	1921.84	1921.40

Crystal Structure of S. aureus-fluorinated Proteins—Replacement of Phe with the fluorinated analog F-F$_5$ should destabilize cation-π interactions. To test this we took advantage of the observation that an intramolecular cation-π interaction between Phe-249 and His-258 is seen in wild type *S. aureus* PI-PLC crystallized under acidic conditions (10). The structure of F249F-F$_5$ was solved and compared with the structure for wild type obtained under acidic pH conditions (structure statistics are presented in Table 3). Electron density is contoured to 1σ for the aromatic residues near the mutation in Fig. 2*A* to show the quality of the data. The cation-π interaction between Phe-249 and the cationic His-258 has a planar stacking distance of 3.5–4.3 Å between the aromatic rings (10). With the F-F$_5$ introduced at position 249, the cation-π complex can no longer form (Fig. 2*C*), and overall F249F-F$_5$ adopts a conformation similar to found in wild type crystallized at basic pH, where His-258 is no longer protonated (10). However, the mobile loop preceding helix G is in a slightly different orientation. The exact disposition of this loop, variable in many of the *S. aureus* mutant crystal structures (10–12), is near protein contacts in the F249F-F$_5$ crystal. This specific orientation of the loop for F249F-F$_5$ likely aids in stabilizing the more hydrophobic F-F$_5$ side chain in the crystal (Fig. 3).

TABLE 3

Full refinement and model statistics for F249F-F$_5$ and H258F-F$_5$ structures

r.m.s.d., root mean square deviation.

	F249F-F$_5$ (PDB 4S3G)	H258F-F$_5$ (PDB 4RV3)
Diffraction data		
Resolution range (Å)	42.26-2.5	49.87-2.0
No. of reflections	12,823	22,307
No. of reflections in free set	623	1139
Space group	$P4_32_12$	$P4_32_12$
Unit cell		
a (Å)	60.05	59.85
b (Å)	60.05	59.85
c (Å)	191.33	180.41
Completeness	99.7	96.6
R_{merge}	0.053	0.056
Refinement		
R_{cryst} [a]	0.212	0.180
R_{free} [b]	0.291	0.238
No. of residues	301	302
No. of non-hydrogen protein atoms	2,408	2,433
No. of H_2O molecules	54	161
No. of non-hydrogen inositol atoms	12	12
No. of ions	1	1
r.m.s.d. bonds (Å)	0.010	0.007
r.m.s.d. bonds angles (degree)	1.337	1.020
Average B-factor (Å^2)	49.0	29.0

[a] $R_{work} = \{\sum \| F_o| - |F_c\|)/|F_o|\}$, where $|F_o|$ and $|F_c|$ are the observed and calculated structure factor amplitudes, respectively.

[b] R_{free} is calculated from a set of 5% randomly selected reflections that were excluded from the refinement.

H258F-F$_5$ was also crystallized under acidic conditions; Fig. 2*B* provides an example of the electron density. Because His-258 has been replaced, the intramolecular cation-π interaction between residues 258 and Phe-249 cannot form. Therefore, in this variant the rim loop containing Phe-249 adopts a conformation close to that seen for H258Y (10) (Fig. 2*D*) that also cannot form the intramolecular cation-π complex. More importantly, the Tyr at residue 258 is nearly superimposable with the F-F$_5$, indicating that introduction of the fluorinated amino acid has virtually no effect on helix G. These structures show that the electrostatics of the fluorinated Phe preclude formation of cation-π complexes and have little effect on the well defined secondary structure in which they may reside.

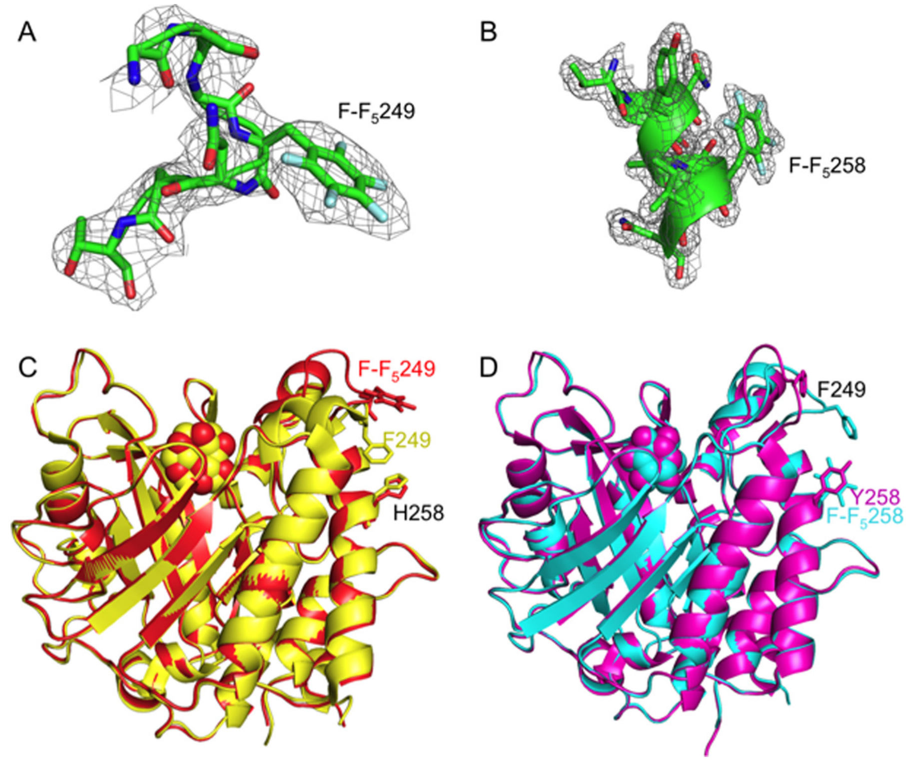

FIGURE 2. Representative electron densities of part of the rim loop in the mutant F249F-F_5 (*A*) and part of the helix G in the mutant H258F-F_5 (*B*) structures are shown in *gray* and contoured at 1σ. Overlay of the pH 4.6 structures for wild type (*yellow*, PDB code 3V16) and F249F-F_5 (*red*, PDB code 4S3G) (*C*) and H258Y (*magenta*, PDB code 3V1H) and H258F-F_5 (*cyan*, PDB code 4RV3) *S. aureus* PI-PLC (*D*) . Key residues are labeled. *myo*-inositol is depicted in space-filling representation.

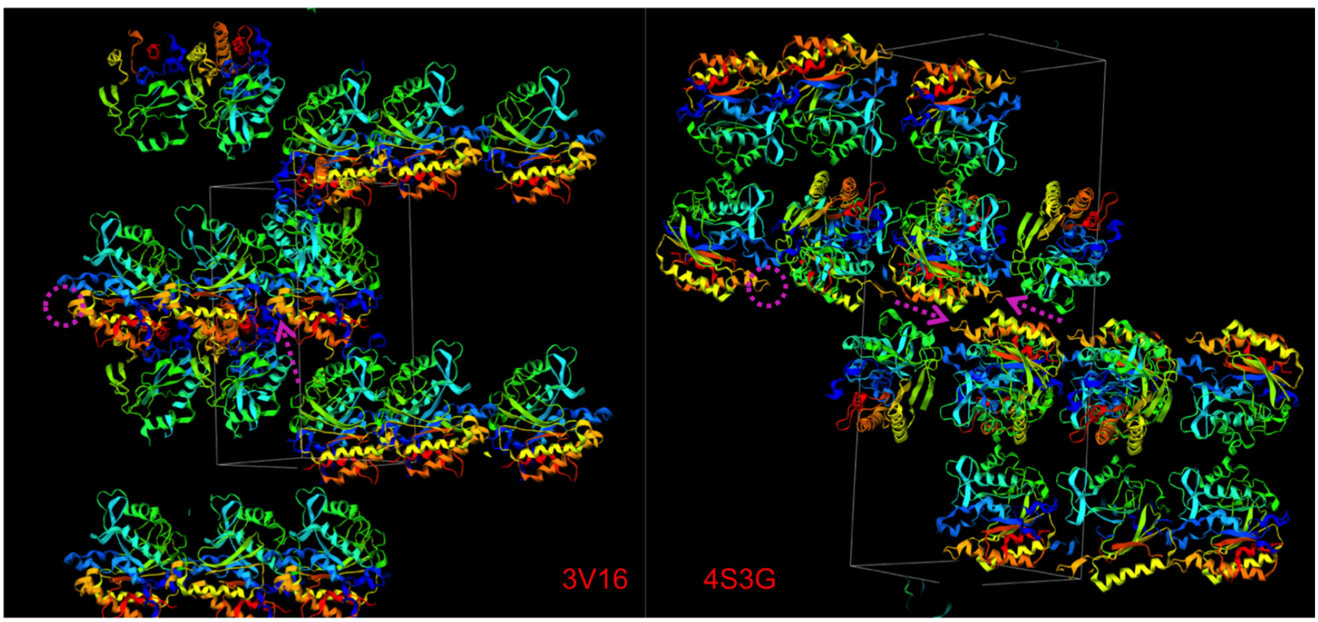

FIGURE 3. **Crystal packing for wild type (PDB code 3V16) and the F249F-F_5 variant (PDB code 4S3G) PI-PLC enzymes.** The rim loop region containing residue Phe or F-F_5 at position 249 is circled in *magenta* and indicated with *arrows* in the respective unit cells. Notice that the hydrophobic residue in the rim loop affects monomer packing in the crystal.

S. aureus Fluorinated PI-PLC Binding to Vesicles—Binding of *S. aureus* PI-PLC variants to PG/PC SUVs was monitored by FCS at pH 6.5 where *S. aureus* PI-PLC shows maximal activity. Wild type protein has weak affinity for PC, and the apparent K_d increases substantially as X_{PC} increases (Fig. 4*A*, *open circles*). Replacing Phe-249 with F-F_5 enhances binding for all vesicle compositions (Fig. 4*A*, *filled circles*). This enhancement is emphasized by plotting the ratio of the apparent K_d for F249F-F_5 relative to that of wild type (Fig. 4*D*). The increased affinity of F249F-F_5 for all vesicle compositions correlates with partitioning of the more hydrophobic F-F_5 into the bilayer.

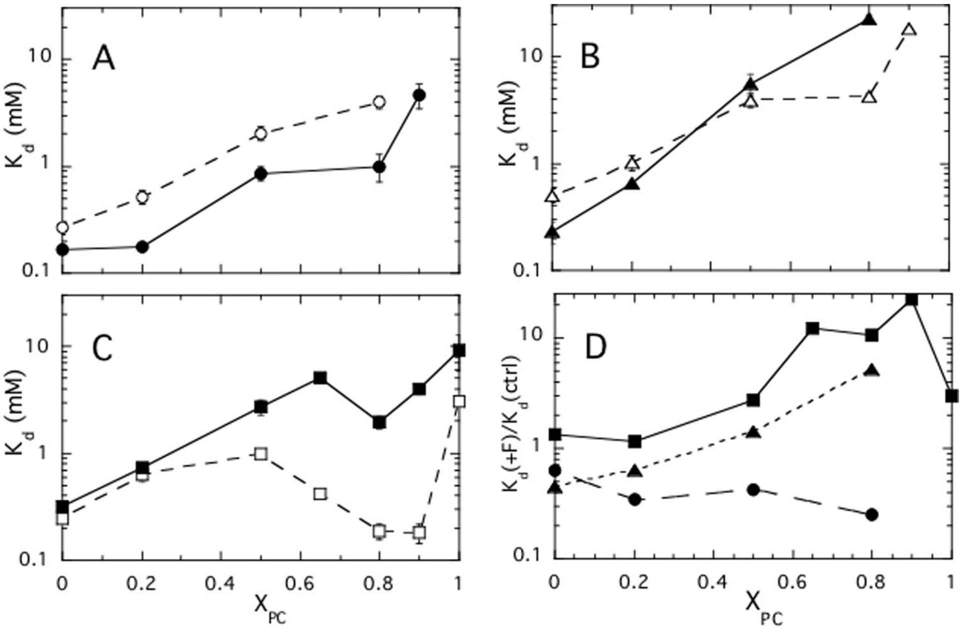

FIGURE 4. **Effects of the fluorinated aromatic amino acids on binding to PG/PC SUVs.** Apparent dissociation constants for *S. aureus* PI-PLC variants containing fluorinated aromatic amino acids as a function of mole percent PC (X_{PC}) for F249F-F_5 (●) compared with wild type (○) (*A*), H258F-F_5 (▲) compared with H258F (△) (*B*), and N254Y/H258Y-F_2 (■) compared with N254Y/H258Y (□) (*C*). *D*, the ratio of the K_d for the fluorinated protein to the K_d for the relevant control, shown in the previous panels, as a function of X_{PC}; symbols are the same as in *A–C*.

The affinity of H258F for the SUVs is comparable with that of the wild type protein (within a factor of two across the range of phospholipid compositions). The binding of H258F-F_5 compared with H258Y (Fig. 4*B*) is similar for $X_{PC} \leq 0.5$. However, at high X_{PC}, H258F-F_5 binding is 5-fold weaker than H258F. At $X_{PC} = 0.9$, the affinity of H258F-F_5 for SUVs was too low to reliably measure by FCS. Thus, although wild type has low affinity for PC-rich membranes, its affinity is further reduced by F-F_5 incorporation in helix G. Because structurally H258F-F_5 is very similar to H258Y, the loss of affinity at high X_{PC} suggests that there is some tendency for a Phe residue introduced at position 258 in the membrane binding interface to interact with choline headgroups. Formation of such a weak complex would require significant PC in the bilayer.

N254Y/H258Y, as reported previously, shows a dramatic increase in affinity for PC-rich SUVs indicative of the introduction of a PC site with these mutations (12). As the PC content increases above $X_{PC} = 0.5$, tight binding of N254Y/H258Y is observed (Fig. 4*C*, *open circles*). The shape of the curve is consistent with a PC cation/Tyr-π interaction contributing to binding in the PC-rich region and electrostatic interactions dominating binding to more anionic PG-rich vesicles. Rather than introduce F-F_5 at this position, we chose to incorporate Y-F_2. However, substituting Y-F_2 for a surface tyrosine can also alter the electrostatic distribution because the Y-F_2 hydroxyl pK_a is shifted to ~7.5 (27). *S. aureus* PI-PLC activity is optimal at pH 6.5, and the binding was measured at that pH. Therefore, deprotonation of the hydroxyl should not interfere significantly with the binding. For the most anionic SUVs, where introduction of a negative charge on the protein should have the strongest effect on binding ($X_{PC} = 0$ and 0.2), the K_d for N254Y/H258Y-F_2 is the same as that for N254Y/H258Y (Fig. 4*C*).

As SUVs become enriched in PC, N254Y/H258Y-F_2 loses much of the binding affinity compared with N254Y/H258Y. This is easily seen from plotting the ratio of K_d for N254Y/H258Y-F_2 to that of its control N254Y/H258Y (Fig. 4*D*). From this ratio we can estimate the free energy lost when substituting Y-F_2 for Tyr. At $X_{PC} = 0.65$, 0.8, and 0.9, $\Delta\Delta G$ values are +6.1, +5.7, and +7.6 kJ/mol, respectively. This very dramatic loss of affinity is consistent with the role of Tyr-258 in cation-π complexes with choline headgroups (12).

Interestingly, for pure PC SUVs, $\Delta\Delta G$ is +2.7 kJ/mol when the Tyr is fluorinated. The lower $\Delta\Delta G$ and the fact that N254Y/H258Y-F_2 binding could still be measured toward pure PC vesicles might suggest that the cation-π interactions have been weakened. Perhaps this is not surprising as only two fluorine atoms were incorporated into the ring. However, another interpretation is that the large $\Delta\Delta G$ values for N254Y/H258Y-F_2 binding to SUVs with some PG indicate that the cation-π complex requires PG binding, likely in the active site as it is a competitive inhibitor, for optimal formation.

Enzyme Activity of Fluorinated S. aureus PI-PLC—With the exception of the pure PI SUVs, enzymatic activities for all the *S. aureus* PI-PLC variants were measured under conditions where the total amount of phospholipid is significantly above the apparent K_d measured by FCS for PG/PC SUVs. Thus, nearly all the proteins should partition onto the vesicles. For all of the variants specific activities increase with increasing PC content (Fig. 5). For wild type this is not due to a specific PC interaction but rather because anionic lipids antagonize dimerization, and *S. aureus* PI-PLC dimers appear to have increased activity (11). For this PI-PLC, zwitterionic phospholipids reduce the surface concentration of PI, and this in turn prevents anionic phospholipids from binding to a cationic site adjacent to the active site that antagonizes dimerization (11). Therefore, all variants exhibited higher activities with increasing X_{PC}.

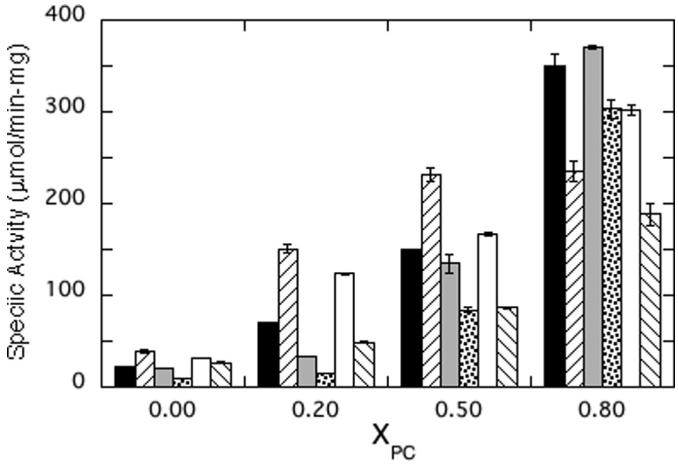

FIGURE 5. **Specific activities of *S. aureus* PI-PLC mutants toward PI/PC SUVs as a function of mole fraction PC (X_{PC}): wild type (■), F249F-F5 (/), H258F (*light gray bars*), H258F-F_5 (·), N254Y/H258Y (□), and N254Y/H258Y-F2 (\).** PI was fixed at 4 mM with increasing amounts of PC. Protein concentrations were adjusted to 0.3–4 μg/ml to ensure <20% cleavage of the PI (4 mM).

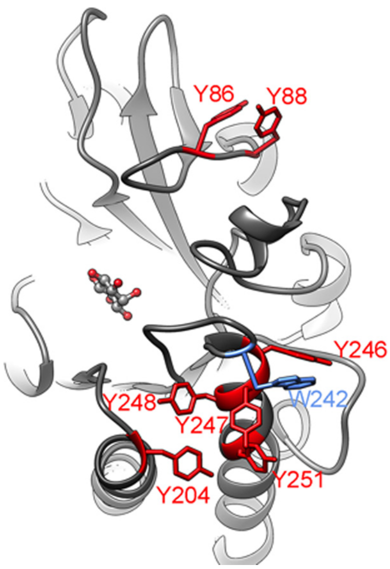

FIGURE 6. **View of *B. cereus* PI-PLC (PDB 1ptg (30) showing the aromatic residues in the area that interacts with the membrane.** *Blue* highlights the loop with Trp-242, which is critical for membrane insertion. *Red* highlights all the tyrosine residues in this region that may be involved in PC cation-aromatic π interactions. An inositol molecule is shown occupying the active site. The *Bacillus cereus* and *B. thuringiensis* PI-PLC sequences are 97% identical, and the membrane binding interface is totally conserved. There is no existing structure for wild type *B. thuringiensis* PI-PLC.

However, superimposed on this behavior are some interesting trends. F249F-F_5 had higher activity than wild type toward PI in vesicles with $X_{PC} \leq 0.5$ (Fig. 5). This increased activity for F249F-F_5 correlates with increasing the hydrophobicity of a side chain that partitions into the membrane, perhaps enhancing processive catalysis on these vesicles. It should be noted that the specific activity decreased at $X_{PC} = 0.8$. Although the exact cause of this is not known, it parallels what is observed for *B. thuringiensis* PI-PLC, where the specific activity drops at high mole fraction of PC where the vesicle binding is tight (5). The affinity of the substrate for the active site depends on the mole fraction of substrate in the interface, its ability to diffuse to the bound enzyme active site, and also the ability of the substrate to dissociate from one vesicle to find another (on the time scale of these assays, the enzyme has to sample many vesicles for ~10% hydrolysis). The tighter binding fluorinated Phe could perturb any of these steps.

With one exception (H258F-F_5, which has very weak binding at $X_{PC} = 0.8$), the total phospholipid concentration used at each X_{PC} was above the apparent K_d for binding to PG/PC SUVs. The fraction of fluorinated protein bound to SUVs can be compared with that of its control protein at each X_{PC}. That ratio is 1.00 ± 0.10. In contrast, the specific activities for these paired enzymes toward vesicles containing PC show larger changes (excluding F249F-F_5 and H258F-F_5 at $X_{PC} = 0.8$). The average ratio of smaller to larger specific activity value is 0.55 ± 0.13. The bigger change for enzyme activities suggests that under conditions where the bulk of the protein is partitioned onto the vesicles, PC cation-protein π interactions in H258F and N254Y/H258Y must also enhance either substrate access or hydrophobic product exit from the active site of the anchored protein. Similarly, increasing the hydrophobic interaction with F249F-F_5 increases the specific activity, and this must reflect a step once the protein is partitioned onto the vesicles.

Y-F_2 in B. thuringiensis PI-PLC Identifies PC Cation-Tyr π Interactions—Given the success in using fluorinated aromatic amino acid incorporation to distinguish side chain partitioning into a bilayer from PC cation-π interactions, we extended this methodology to *B. thuringiensis* PI-PLC. This PI-PLC has a large number of Tyr residues in rim loops as well as in helix G that could interact with the bilayer (Fig. 6). Recent MD simulations have suggested transient cation-π complexes exist when the protein is bound to a PC bilayer (6). Experimental tests to see which Tyr residues were critical for membrane binding substituted the Tyr with Ala. This substitution impaired binding if the mutated Tyr partitioned into the bilayer. However, the Ala mutations only indicate which residues are important for membrane binding, not the mode of binding.

To investigate how *B. thuringiensis* PI-PLC Tyr residues interact with phospholipids, we constructed seven Y-F_2 variants (Y86Y-F_2, Y88Y-F_2, Y204Y-F_2, Y246Y-F_2, Y247Y-F_2, Y248Y-F_2, and Y251Y-F_2) and examined their binding to PG and PC SUVs at pH 7.4, the optimal pH for the activity of this enzyme. At this pH the hydroxyl group of each surface Y-F_2 will be ~50% ionized introducing a partial negative charge in the vicinity of the bilayer. That is likely to affect the affinity of the proteins for PG surfaces (quantified by the K_d for pure PG SUVs) but have only a modest effect on binding to a zwitterionic bilayer (pure PC SUVs). For the latter, a reduction in K_d would indicate nonspecific partitioning of that Tyr into the bilayer, *i.e.* interactions with lipid tails, whereas an increase in K_d would indicate participation in PC cation-π binding. A summary of the apparent K_d values obtained by FCS are shown in Table 4.

Successful incorporation of Y-F_2 into all variants was confirmed by fluorine NMR (data not shown). All Y-F_2 variants show impaired binding to PG SUVs with the apparent K_d increasing from 5.6 mM for wild type to 30–40 mM for the fluorinated proteins. The average $\Delta\Delta G$ for these Y-F_2 variants binding to PG SUVs, +4.4 ± 0.5 kJ/mol, represents the electro-

TABLE 4
Apparent K_d value for *B. thuringiensis* PI-PLC Y→Y-F_2 mutants and extrapolated ΔΔG for loss of binding

PI-PLC	PG SUVs K_d	ΔΔG (PG)[a]	PC SUVs K_d	ΔΔG (PC)[a]	% Occupancy cation-π[b]	PC SUVS, Y→A[b] K_d
	mM		*mM*			*mM*
WT	5.60 ± 0.04		0.030 ± 0.006			
Y86Y-F_2	41.2 ± 1.2	4.9	0.62 ± 0.03	7.4	22	0.072 ± 0.005
Y88Y-F_2	30.3 ± 1.5	3.6	0.78 ± 0.07	8.0	96	1.2 ± 0.3
Y204Y-F_2	36.9 ± 5.5	4.7	1.04 ± 0.06	8.7	26	0.87 ± 0.58
Y246Y-F_2	34.5 ± 10.1	4.5	1.09 ± 0.02	8.8	77	1.2 ± 0.3
Y247Y-F_2	28.2 ± 1.4	4.0	0.053 ± 0.004	1.4	8.9	0.082 ± 0.007
Y248Y-F_2	40.2 ± 9.4	4.9	2.31 ± 0.07	10.6	1.9	2.5 ± 0.5
Y251Y-F_2	28.7 ± 8.6	4.0	0.69 ± 0.46	7.7	36	0.8 ± 0.4

[a] Extrapolated from the ratio of K_d(mutant)/K_d(WT) at 22 °C.
[b] Y→A is the mutant PI-PLC with alanine in the place of the Tyr at that position. These binding data are from Grauffel *et al.* (6).

static cost of placing a fluorinated ring (and partial negative charge) at an anionic interface.

In contrast to the uniform behavior of these variants with a PG vesicle, the apparent K_d values for pure PC SUVs covered a much wider range. The Y247Y-F_2 K_d was <2-fold higher than that of wild type *B. thuringiensis* PI-PLC, indicating as suggested from previous experiments and MD simulations (6) that Tyr247 does not contribute significantly to cation-π interactions. The largest increase in the apparent K_d for PC containing vesicles was observed for Y248Y-F_2 (from 0.03 to 2.3 mM). However, the MD simulations strongly suggest this is not because of cation-π interactions but rather arises from intramolecular interactions. Tyr-248 in the rim loop helps properly position Trp-242 (6), and this Trp is very important for membrane binding. All mutations to Tyr-248 appear to disrupt this interaction.

Y204Y-F_2 and Y246Y-F_2 show the next largest increases in K_d followed by Y86Y-F_2, Y88Y-F_2, and Y251Y-F_2. In the MD simulations, all of these Tyr residues contribute to cation-π interactions but with different occupancies. The apparent K_d values for the Y-F_2 variants also correlate well with those for the alanine variants (Table 4). For both there is a qualitative correlation of the loss of binding affinity with cation-π occupancy observed in the MD simulations.

The important observation is that none of the K_d values for Y-F_2 variants binding to PC SUVs decreased. Therefore, for this PI-PLC, the surface Tyr residues do not partition into the membrane but rather engage in cation-π interactions to different degrees. For PC-rich bilayers, cation-π interactions are ideal for transiently anchoring these proteins long enough to search an initial area for their glycosylphosphatidylinositol-anchored substrates to cleave ~10 substrates followed by hopping to a new region on the PC-rich outer plasma membrane (28).

This approach using fluorinated amino acids to distinguish the type of membrane interaction of a particular aromatic side chain should have broad applicability to many other systems. Integral membrane proteins have aromatic residues at the membrane surface, and these may also engage in cation-π interactions with the membrane. For example, PC modulation of an aspartate transporter from *Pyrococcus horikoshii* is postulated to occur through a cation-π interaction with a surface Tyr and the lipid headgroup. In that case, the interaction influences conformational flexibility of the oligomerization domain, which in turn modulates the rate of transport (29). Use of Y-F_2 in such a system could provide direct evidence for such a cation-π interaction.

Summary—The incorporation of fluorinated amino acids into these two amphitropic proteins has allowed us to assess directly how specific aromatic amino acids interact with membranes. This approach should be useful in providing a direct test of predictions from MD simulations and in designing membrane binding interfaces based on PC cation-protein π interactions. Thus, this methodology is broadly applicable to proteins that interact with membranes and can provide new insight into the roles of specific aromatic amino acids in membrane-protein interactions.

Author Contributions—T. H. created and characterized all *S. aureus* and *B. thuringiensis* variants. S. E. carried out the MS experiments. Y.-J. L. and W. L. generated the pEVOL-pylT-PylRS system for incorporation of F-F_5. J. W. generated the pEVOL-F2YRS system for incorporation of Y-F_2 into proteins. J. G. helped with the synthesis of Y-F_2 and interpretation of the binding data. T. H. and M. R. planned experiments and wrote the manuscript along with A. G., who also supervised FCS experiments. All authors reviewed the results and approved the final version of the manuscript.

References

1. Lemmon, M. A. (2008) Membrane recognition by phospholipid-binding domains. *Nat. Rev. Mol. Cell Biol.* **9,** 99–111
2. Kutateladze, T. G. (2010) Translation of the phosphoinositide code by PI effectors. *Nat. Chem. Biol.* **6,** 507–513
3. Krick, R., Busse, R. A., Scacioc, A., Stephan, M., Janshoff, A., Thumm, M., and Kühnel, K. (2012) Structural and functional characterization of the two phosphoinositide binding sites of PROPPINs, a β-propeller protein family. *Proc. Natl. Acad. Sci. U.S.A.* **109,** E2042–E2049
4. Karathanassis, D., Stahelin, R. V., Bravo, J., Perisic, O., Pacold, C. M., Cho, W., and Williams, R. L. (2002) Binding of the PX domain of p47(phox) to phosphatidylinositol 3,4-bisphosphate and phosphatidic acid is masked by an intramolecular interaction. *EMBO J.* **21,** 5057–5068
5. Pu, M., Roberts, M. F., and Gershenson, A. (2009) Fluorescence correlation spectroscopy of phosphatidylinositol-specific phospholipase C monitors the interplay of substrate and activator lipid binding. *Biochemistry* **48,** 6835–6845
6. Grauffel, C., Yang, B., He, T., Roberts, M. F., Gershenson, A., and Reuter, N. (2013) Cation-π interactions as lipid-specific anchors for phosphatidylinositol-specific phospholipase C. *J. Am. Chem. Soc.* **135,** 5740–5750
7. Pu, M., Orr, A., Redfield, A. G., and Roberts, M. F. (2010) Defining specific lipid binding sites for a peripheral membrane protein *in situ* using subtesla field-cycling NMR. *J. Biol. Chem.* **285,** 26916–26922
8. Pace, C. J., and Gao, J. (2013) Exploring and exploiting polar-π interactions with fluorinated aromatic amino acids. *Acc. Chem. Res.* **46,** 907–915
9. Dougherty, D. A. (2013) The cation-π interaction. *Acc. Chem. Res.* **46,** 885–893
10. Goldstein, R., Cheng, J., Stec, B., and Roberts, M. F. (2012) Structure of the *S. aureus* PI-specific phospholipase C reveals modulation of active site

access by a titratable π-cation latched loop. *Biochemistry* **51,** 2579–2587
11. Cheng, J., Goldstein, R., Stec, B., Gershenson, A., and Roberts, M. F. (2012) Competition between anion binding and dimerization modulates *Staphylococcus aureus* phosphatidylinositol-specific phospholipase C enzymatic activity. *J. Biol. Chem.* **287,** 40317–40327
12. Cheng, J., Goldstein, R., Gershenson A., Stec, B., and Roberts M. F. (2013) The cation-π box is a specific phosphatidylcholine membrane targeting motif. *J. Biol. Chem.* **288,** 14863–14873
13. Seyedsayamdost, M. R., Yee, C. S., and Stubbe, J. (2007) Site-specific incorporation of fluorotyrosines into the R2 subunit of *E. coli* ribonucleotide reductase by expressed protein ligation. *Nat. Protoc.* **2,** 1225–1235
14. Li, F., Shi, P., Li, J., Yang, F., Wang, T., Zhang, W., Gao, F., Ding, W., Li, D., Li, J., Xiong, Y., Sun, J., Gong, W., Tian, C., and Wang, J. (2013) A genetically encoded ^{19}F NMR probe for tyrosine phosphorylation. *Angew. Chem. Int. Ed. Engl.* **52,** 3958–3962
15. Young, T. S., Ahmad, I., Yin, J. A., and Schultz, P. G. (2010) An enhanced system for unnatural amino acid mutagenesis in *E. coli*. *J. Mol. Biol.* **395,** 361–374
16. Feng, J., Wehbi, H., and Roberts, M. F. (2002) Role of tryptophan residues in interfacial binding of phosphatidylinositol-specific phospholipase C. *J. Biol. Chem.* **277,** 19867–19875
17. Cheng, J., Karri, S., Grauffel, C., Wang, F., Reuter, N., Roberts, M. F., Wintrode, P. L., and Gershenson, A. (2013) Does changing the predicted dynamics of a phospholipase C alter activity and membrane binding? *Biophys. J.* **104,** 185–195
18. Middleton, E. R., and Rhoades, E. (2010) Effects of curvature and composition on α-synuclein binding to lipid vesicles. *Biophys. J.* **99,** 2279–2288
19. Rusu, L., Gambhir, A., McLaughlin, S., and Rädler, J. (2004) Fluorescence correlation spectroscopy studies of Peptide and protein binding to phospholipid vesicles. *Biophys. J.* **87,** 1044–1053
20. Thompson, N. L. (1991) In *Topics in Fluorescence Spectroscopy* (Lakowicz, J. R., ed.) p. 337, Plenum Press, New York
21. Pflugrath, J. W. (1999) The finer things in x-ray diffraction data collection. *Acta Crystallogr. D Biol. Crystallogr.* **55,** 1718–1725
22. Adams, P. D., Afonine, P. V., Bunkóczi, G., Chen, V. B., Davis, I. W., Echols, N., Headd, J. J., Hung, L. W., Kapral, G. J., Grosse-Kunstleve, R. W., McCoy, A. J., Moriarty, N. W., Oeffner, R., Read, R. J., Richardson, D. C., Richardson, J. S., Terwilliger, T. C., and Zwart, P. H. (2010) PHENIX: a comprehensive Python-based system for macromolecular structure solution. *Acta Crystallogr. D Biol. Crystallogr.* **66,** 213–221
23. McCoy, A. J., Grosse-Kunstleve, R. W., Adams, P. D., Winn, M. D., Storoni, L. C., and Read, R. J. (2007) Phaser crystallographic software. *J. Appl. Crystallogr.* **40,** 658–674
24. Emsley, P., and Cowtan, K. (2004) Coot: model-building tools for molecular graphics. *Acta Crystallogr. D Biol. Crystallogr.* **60,** 2126–2132
25. Krissinel, E., and Henrick, K. (2004) Secondary-structure matching (SSM), a new tool for fast protein structure alignment in three dimensions. *Acta Crystallogr. D Biol. Crystallogr.* **60,** 2256–2268
26. DeLano, W. L. (2010) *The PyMOL Molecular Graphics System*, Version 1.3. Schrodinger, LLC, New York
27. Ravichandran, K. R., Liang, L., Stubbe, J., and Tommos, C. (2013) Formal reduction potential of 3,5-difluorotyrosine in a structured protein: insight into multistep radical transfer. *Biochemistry* **52,** 8907–8915
28. Yang, B., Pu, M., Khan, H. M., Friedman, L., Reuter, N., Roberts, M. F., and Gershenson, A. (2015) quantifying transient interactions between *Bacillus* phosphatidylinositol-specific phospholipase C and phosphatdoylcholine0rich vesicles. *J. Am. Chem. Soc.* **137,** 14–17
29. McIlwain, B. C., Vandenberg, R. J., and Ryan, R. M. (2015) Transport rates of a glutamate transporter homologue are influenced by the lipid bilayer. *J. Biol. Chem.* **290,** 9780–9788
30. Heinz, D. W., Ryan, M., Bullock, T. L., and Griffith, O. H. (1995) Crystal structure of the phosphatidylinositol-specific phospho-lipase C from *Bacillus cereus* in complex with *myo*-inositol. *EMBO J.* **14,** 3855–3863

Membrane Biology:
Fluorinated Aromatic Amino Acids Distinguish Cation- π Interactions from Membrane Insertion

Tao He, Anne Gershenson, Stephen J. Eyles, Yan-Jiun Lee, Wenshe R. Liu, Jiangyun Wang, Jianmin Gao and Mary F. Roberts

J. Biol. Chem. 2015, 290:19334-19342.
doi: 10.1074/jbc.M115.668343 originally published online June 19, 2015